Adapting to Extreme Heat: Social, Atmospheric, and Infrastructure Impacts of Air-Conditioning in Megacities—The Case of New York City

Harold Gamarro
Department of Mechanical Engineering,
The City College of New York,
New York, NY 10031
e-mail: hgamarr00@citymail.cuny.edu

Luis Ortiz
Urban Systems Lab,
The New School,
New York, NY 10011
e-mail: ortizl@newschool.edu

Jorge E. González[1]
Department of Mechanical Engineering,
The City College of New York,
New York, NY 10031
e-mail: jgonzalezcruz@ccny.cuny.edu

Extreme heat events are becoming more frequent and intense. In cities, the urban heat island (UHI) can often intensify extreme heat exposure, presenting a public health challenge across vulnerable populations without access to adaptive measures. Here, we explore the impacts of increasing residential air-conditioning (AC) adoption as one such adaptive measure to extreme heat, with New York City (NYC) as a case study. This study uses AC adoption data from NYC Housing and Vacancy Surveys to study impacts to indoor heat exposure, energy demand, and UHI. The Weather Research and Forecasting (WRF) model, coupled with a multilayer building environment parameterization and building energy model (BEP–BEM), is used to perform this analysis. The BEP–BEM schemes are modified to account for partial AC use and used to analyze current and full AC adoption scenarios. A city-scale case study is performed over the summer months of June–August 2018, which includes three different extreme heat events. Simulation results show good agreement with surface weather stations. We show that increasing AC systems to 100% usage across NYC results in a peak energy demand increase of 20%, while increasing UHI on average by 0.42 °C. Results highlight potential trade-offs in extreme heat adaptation strategies for cities, which may be necessary in the context of increasing extreme heat events. [DOI: 10.1115/1.4048175]

Keywords: air-conditioning, building, urban climate, regional climate model, sustainability

1 Introduction

Extreme heat events are becoming more frequent and intense worldwide. According to the Intergovernmental Panel on Climate Change (IPCC) report [1], the risk of heatwaves will increase during the twenty-first century, requiring adaptation measures to reduce impacts on health and comfort, particularly in vulnerable populations like the elderly and low-income communities [2,3]. The 2020 New York City Panel on Climate Change (NPCC) also reported that summer heat waves are expected to become more frequent, longer, and more intense in New York City (NYC), the largest city in the US [4]. The Urban Heat Island (UHI) has been shown to further exacerbate this problem in cities, which tend to have higher ambient temperatures than the surrounding regions [5,6]. The UHI effect is a result of how built-up areas modify land-air processes as a result of high heat capacity materials, high density of vertical structures with varying heights, limited green spaces, and anthropogenic heat release [7–9]. This UHI may intensify periods of extreme heat locally due to a lack of surface moisture in urban areas, low wind speed associated with heat waves, and increased heat storage and generation [6,10–15]. As a result, these intensified heatwaves are projected to cause an increased demand in air-conditioning (AC) [16,17] with a rise in global AC ownership of about two-thirds of all households by 2050 [18]. Furthermore, around 55% of the world's population currently reside in urban areas. This is projected to increase to 68% by 2050 [19,20], further increasing the health and economic risks associated with intense heat waves.

Higher urban ambient temperatures present challenges that are likely to cause social, environmental, and infrastructural impacts. For instance, urban overheating will cause an increase in energy demand for space cooling, with global residential cooling energy demand projected to increase between 320% (low development scenario) and 2270% (high development scenario) [21]. Urban overheating will also have a drastic impact on the most vulnerable populations in the cities in terms of health and comfort. In NYC, premature mortality is projected to grow between 47% and 95% by mid-century as a result of heat waves [22]. Lower income and vulnerable populations, like the elderly, experience disproportionally higher heat-related mortality rates [2,23,24]. One reason to explain this disparity can be a result of a building envelope with low thermal quality that presents significant overheating [25,26]. Another reason can be the low prevalence of AC as reported by O'Neil et al. [27] and Ito et al. [28], who also found that areas with lower AC adoption coincide with higher rates of heat-related mortality and hospitalizations. As a result, the most vulnerable will be exposed to higher indoor temperatures while also needing more energy than the average to fully meet the cooling demand [26] ultimately bearing a higher energy cost burden [29].

In this investigation, we explore the overall impacts of increasing AC system adoption in residences to 100% as an adaptive measure to reduce human health risks under heat waves, with NYC as a case study. To account for the interaction between weather, buildings, and energy demand, an urbanized version of the Weather and Research Forecasting (WRF) [30] model is used. This urbanized model couples WRF to a multilayer building environment parameterization and building energy model (BEP–BEM) that has been

[1]Corresponding author.

Manuscript received May 31, 2020; final manuscript received August 14, 2020; published online September 9, 2020. Assoc. Editor: Shiguang Miao.

used extensively to study urban climate and energy demand [31–37]. In particular, Takane et al. [35] found that the base configuration of BEP–BEM significantly overestimated the electricity demand in Osaka City, a megacity located in Japan. This is due to the assumption of BEP–BEM that all spaces inside the building undergo air-conditioning. To correct this error, the authors introduced three new constant parameters (a - ratio of in-use building to all buildings, b - ratio of air-conditioned floor area to total floor area, and c - the ratio of AC usage for cooling or heating to all the cooling and heating equipment) to consider the use of partial AC systems in the model leading to improvements in both the surface temperature and electricity demand outputs of the model. Xu et al. [37] reported similar results over Beijing, China, but instead introduced a constant cool fraction parameter as a function of urban land class. These developments were found to significantly improve the AC electric load on a district level when compared to observation data.

In this study, we introduce AC adoption data from the 2017 New York City Housing and Vacancy Surveys to study the impacts of full AC adoption to indoor heat exposure, energy demand, and UHI within the urbanized WRF framework.

2 Methods

2.1 Experimental Design. Three case setups were used to evaluate the social, environmental, and infrastructural implications of increasing residential AC adoption to 100%. Each of these cases used a fully resolved urbanized WRF setup with differences in the AC adoption percentage input data used as input to the building energy model. The first case, referred to onward as the NO_AC case, simulates a 0% adoption scenario to model potential indoor health exposure throughout the city. The second case, referred to onward as the CURRENT_AC adoption case, used data from the NYC Housing and Vacancy Survey 2017 to represent the current AC adoption rate in NYC as shown in Fig. 1 highlighting the percentage of households with AC. The final case, referred to onward as the Full_AC adoption case, represents the 100% AC adoption case in NYC with the assumption that the AC was used to cool each building to maintain a set temperature of 22.22 °C. The second and third cases were used to explore the differences on impacts using the CURRENT_AC case as the baseline setup that closely represents NYC. A summary of these cases is shown in Table 1.

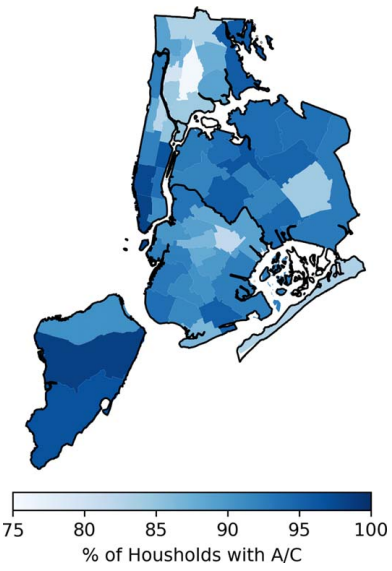

Fig. 1 AC % data: 2017 New York City Housing and Vacancy Survey data of households with AC in terms of percentage

Table 1 Numerical experiments performed in this study

Case	Description of case
NO_AC	Case associated with regions that currently have no AC using 0% AC data in the model
CURRENT_AC	Case representing the current AC adoption rate in NYC using data from the NYC Housing and Vacancy Survey 2017
FULL_AC	Case representing full AC adoption in NYC using 100% AC data in the model

2.2 Urbanized Weather and Research Forecasting Description. WRF is a non-hydrostatic mesoscale numerical weather prediction (NWP) system used for weather-related research and forecasting [30]. Mesoscale meteorological models provide the capability to explore these questions using a detailed model representation of the atmosphere and the city that can compute the conservation equations of mass, momentum, energy, and air humidity [30]. At the mesoscale, many processes affect how the atmospheric circulation is resolved. This includes the interaction of the land-use type and surface characteristics, complex topography, water bodies and atmospheric composition. In cities, the urban canopy can also significantly influence the dynamical state of the environment. Urban areas, characterized by significant building area coverage, high density of vertical surfaces with varying heights, and high heat capacity materials, cause surface–atmosphere interactions to differ in comparison with the natural environment. This modified surface energy balance tends to cause the urban areas to be warmer with increases in temperature of up to 10 °C [8,38] leading to the UHI. When coupled with BEP–BEM, the mesoscale model can serve as an appropriate urban climate modeling framework that is proven to capture these unique UHI effects [31,39,40]. Most of the previous urban WRF applications have explored extreme heat events in cities, including for New York City [6,33,40,41], which is the case study of interest of this research.

BEP is a multilayer urban parameterization that models the atmospheric effects caused by urban buildings and includes heat flux adjustments to account for radiation shadowing, reflection, and entrapment within the street canyons [42]. BEM is then coupled with the BEP to account for urban heat fluxes caused by heat exchanges between the buildings and the environment. This includes the heat transfer between the walls, floors, and roofs of a building, the solar radiation heat exchange through windows and the effects of air-conditioning, heating, and ventilation [31].

Within this system, the indoor air temperature and indoor air humidity are found by calculating the cooling/heating load on a simplified box-type heat budget model that pile up like boxes to consider several floors in a building. This model is driven by the inputs of the WRF model like the outdoor air temperature, humidity, and radiation reaching the walls and roof of the building. The indoor air temperature T_r and indoor air humidity q_{vr} are estimated by solving the following equations [31]:

$$Q_B \frac{dT_r}{dt} = H_{in} - H_{out} \tag{1}$$

$$l\rho V_B \frac{dq_{vr}}{dt} = E_{in} - E_{out} \tag{2}$$

where $Q_B = \rho C_p V_B (JK^{-1})$ and $V_B(m^3)$ represent the overall heat capacity and total volume of the indoor air on the floor, respectively. The total sensible heat load $H_{in}(W)$ and total latent heat load $E_{in}(W)$ are computed within the model using WRF inputs mentioned previously. The sensible heat load includes the heat exchange between the indoor air and each component of the building surface like the roof, walls, and windows. It also includes the sensible heat exchange that occurs through ventilation, and finally, the internal

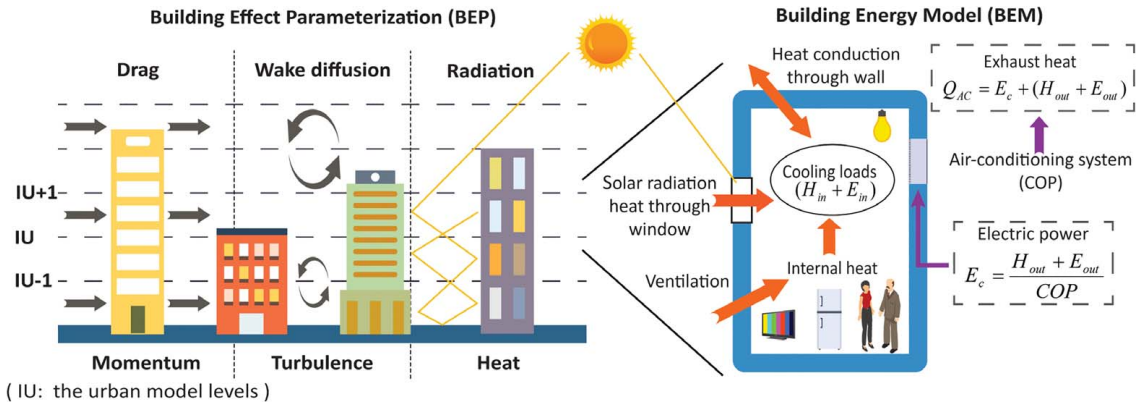

Fig. 2 uWRF BEP–BEM modeling representation

sensible heat that is generated from sources like equipment and occupants. The latent heat load includes the water vapor mixing that occurs from ventilation and considers the component for the evaporation from occupants. The remaining components $H_{out}(W)$ and $E_{out}(W)$ in Eqs. (2) and (3) indicate the sensible and latent heat needed for cooling/heating the indoor air for the floor when a target temperature is set. From this formulation, the electricity demand E_C can then be found using the following equation:

$$E_C = \frac{1}{cop}(H_{out} + E_{out}) \tag{3}$$

This modeling approach makes no distinction between window AC units and central AC systems, with the assumption that all heat releases is at the top of the building. An air-cooled approach is used for the residential land class while the water cooled is used for the commercial land class. Sensible or latent heat partitioning from the AC system then follows the work by Gutierrez et al. [43]. Figure 2 shows a visual representation of this entire built–environment–buildings coupled process. We refer to WRF coupled to BEP + BEM as urban WRF (or uWRF). In general, this framework is a simplified version of more detailed BEMs, such as EnergyPlus [44], but they reduce computational cost and are suitable for studies at the city scale [35]. Model performance of uWRF for city-scale energy demands have been reported for Beijing, China [37], and for New York City [34], with very good results when compared with actual observations.

To obtain the city-scale energy loads from BEM outputs, the gridded 1-km resolution model air-conditioning consumption (W/m^2) was multiplied by the building area fraction and the actual grid spacing area (1 km^2), yielding the total building energy demand per grid point. This was then added to a city-wide baseline load as shown in Fig. 3 which represents the nonbuilding associated loads in NYC. The baseline load was calculated following the approach described by Salamanca et al. [32] and Ortiz et al. [34].

To make use of the BEP/BEM parametrization, sub-grid urban building data sets were required to represent the urban landscape and drive the uWRF model. From these data sets, an urban land-use map was created for three land-use categories including low-intensity residential (LIR), high-intensity residential (HIR), and finally commercial or industrial (COI). In this work, the urban building data set requirements were obtained from the Property Land Use Tax-Lot Output (PLUTO) data set, a resource provided by the NYC municipality through the NYC open data initiative, at a spatial resolution of 100 m. This data was then upscaled to a 1 km × 1 km domain to match the high-resolution WRF domain as shown in Figs. 4(*a*)–4(*c*). This provides the required building height and building area fraction for the NYC region to classify each land class as previously described. Different urban canopy parameters were also prescribed within the BEM. This includes the thermal surface properties of the roof, wall and

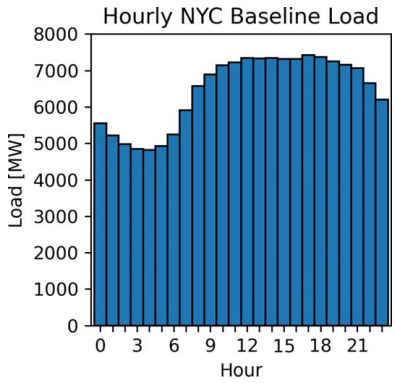

Fig. 3 Baseline city-wide load derived from the NYISO load data

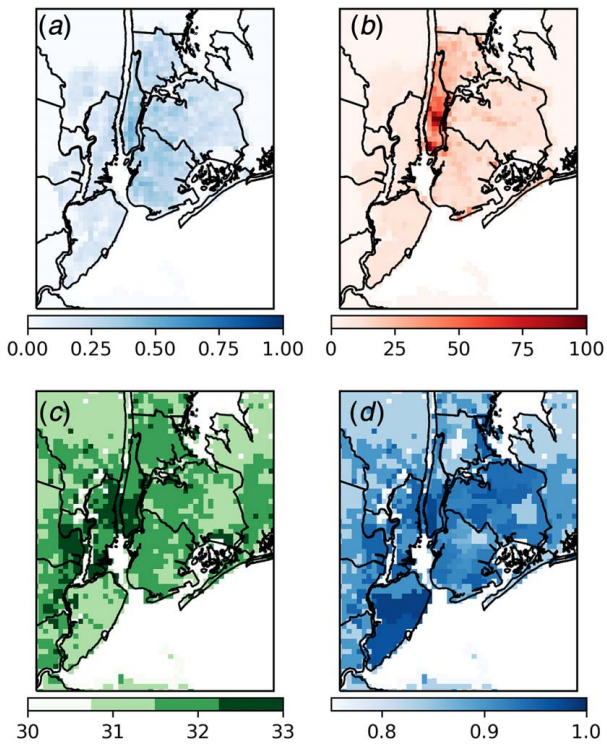

Fig. 4 uWRF model inputs reinterpolated to 1 km WRF domain: (*a*) building area fraction (%), (*b*) building height (m), (c) land-use type, and (*d*) AC distribution (%)

Table 2 Urban parameters used in each uWRF simulation

Parameters	Units	LIR	HIR	COI
Roof heat capacity	$Jm^{-3}K^{-1} \times 10^6$	1.32	1.32	1.32
Roof thermal conductivity	$Jm^{-1}s^{-1}K^{-1}$	0.67	0.67	0.67
Roof albedo		0.2	0.2	0.2
Roof emissivity		0.9	0.9	0.9
Roof insulation thickness	m	0.06	0.06	0.06
Roof insulation heat capacity	$Jm^{-3}K^{-1} \times 10^6$	0.382	0.382	0.382
Roof insulation thermal conductivity	$Jm^{-1}s^{-1}K^{-1}$	0.09	0.09	0.09
Wall heat capacity	$Jm^{-3}K^{-1} \times 10^6$	1.32	1.32	1.32
Wall thermal conductivity	$Jm^{-1}s^{-1}K^{-1}$	0.67	0.67	0.67
Wall albedo		0.2	0.2	0.2
Wall emissivity		0.9	0.9	0.9
Wall insulation thickness	m	0.06	0.06	0.06
Wall insulation heat capacity	$Jm^{-3}K^{-1} \times 10^6$	0.382	0.382	0.382
Wall insulation thermal conductivity	$Jm^{-1}s^{-1}K^{-1}$	0.09	0.09	0.09
Road heat capacity	$Jm^{-3}K^{-1} \times 10^6$	1.4	1.4	1.4
Road thermal conductivity	$Jm^{-1}s^{-1}K^{-1}$	0.74	0.74	0.74
Road albedo		0.125	0.125	0.125
Road emissivity		0.95	0.95	0.95
Temperature set point	°C	22.22	22.22	22.22
Humidity set point	$kgkg^{-1}$	0.01	0.01	0.01
Coefficient of performance of AC		3.5	3.5	3.5
Window area fraction		0.33	0.33	0.33
Peak occupancy	$personm^{-2}$	0.25	0.25	0.05
Initial and end times of AC system	Local time	0–24	0–24	8–19

road and AC model parameters, as summarized in Table 2. The thermal properties were adopted from Salamanca et al. [45] while the AC model parameters follow previous work [43,46].

In this investigation, the BEM within uWRF was modified to include the AC percentage data information from the NYC Housing and Vacancy Survey 2017. This was done by modulating the sensible $H_{out}(W)$ and Latent $E_{out}(W)$ heat fluxes with the specific AC household percentage parameter α as follows:

$$E_c^p = \frac{1}{cop}(H_{out}^p + E_{out}^p) \tag{4}$$

$$H_{out}^p = H_{out} \times \alpha \tag{5}$$

$$E_{out}^p = E_{out} \times \alpha \tag{6}$$

Some preprocessing was performed to re-grid the data from a community district level grouping (Fig. 1) to the 1 km × 1 km domain used in the uWRF model, the results of this exercise can be seen in Fig. 4(*d*).

2.3 Model Setup. Each of the three model cases as shown in Table 1 was set up using WRF v 3.9.1 and configured with three two-way nested domains at horizontal resolutions of 9, 3, and 1 km as shown in Fig. 5. The 1 km × 1 km domain was the primary focus of this investigation, as it is the domain primarily encompassing the NYC region with the highest urban density. Each of these model cases was configured to use the Noah land surface model [47], the Rapid Radiative Transfer Model for Global Circulation Models (RRTMG) for longwave radiation [48], the RRTMG scheme for shortwave radiation [48], the Mellor–Yamada–Janjic planetary boundary layer scheme [49], and the Aerosol aware Thompson microphysics scheme [50]. A summary of the model's physics parameterizations used in this investigation is given in Table 3. The model outputs consist of 0-24-hour forecasts simulated with a time ranging from June 1, 2018 to August 30, 2018. A detail description of the uWRF configuration is given in Ortiz et al. [34].

2.4 Evaluation Methods. Model performance was evaluated against ground station weather data using weather data from the New York State Mesonet network for the summer months of June to August 2018.[2] The CURRENT_AC case was chosen as the model setup to evaluate since it closely represents NYC with the added AC information. Hourly outputs of temperature, wind speed, and wind direction were compared at five different stations in the city's five boroughs (Brooklyn, Bronx, Queens, Staten Island, and Manhattan as shown in Fig. 6) using different suitable performance metrics. These metrics included the root-mean-square error (RMSE), mean absolute error (MAE), and the correlation coefficient (R^2) to measure the degree of error in comparison with the observations. For this evaluation, weekends were excluded as the model only considers a weekday work schedule from Monday to Friday.

2.5 Socioeconomic and Health Impacts. We quantify the present exposure to hazardous heat conditions using the heat index metric [51] that combines both the temperature and relative humidity to quantify the "apparent" temperature a person can experience, making it more representative of indoor human comfort. The NO_AC case was used to estimate the indoor heat index using the uWRF BEM outputs of indoor air temperature and humidity as inputs for the heat index algorithm. The indoor heat index was then calculated following the National Weather Service (NWS) algorithm as outlined by Anderson et al. [52]. Although the NWS heat index was designed for outdoor conditions, in this study it was used as a departure from reference indoor human comfort conditions of 22 °C and 50% relative humidity following American Society of Heating, Refrigeration and Air Conditioning (ASHRAE) standards [53]. The indoor heat index has also been previously used as a metric for indoor human comfort. Vant-Hull et al. [54] studied the impact of indoor residential heat waves in NYC and found that nearly two-thirds of the residences experience elevated heat index conditions compared to the ambient conditions. Uejio et al. [55] used the indoor heat index to conclude that a higher heat index increased the odds of making a respiratory distress call to paramedics in NYC. It has also been used in practice when defining policy that relates to

[2] http://www.nysmesonet.org/

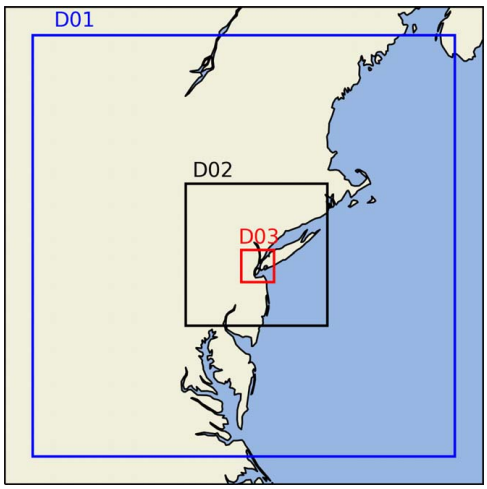

Fig. 5 Model domain: outer (d01) and nested domains (d02, d03) used by the urbanized model

Table 3 Summary of physics parameterization

Model physics	Scheme
Land surface model	NOAH LSM [47]
Longwave radiation	RRTMG [48]
Shortwave radiation	RRTMG [48]
Planetary boundary layer	Mellor–Yamada–Janjic [49]
Microphysics	Aerosol aware Thompson [50]
Urban surface	BEP + BEM [31,42]

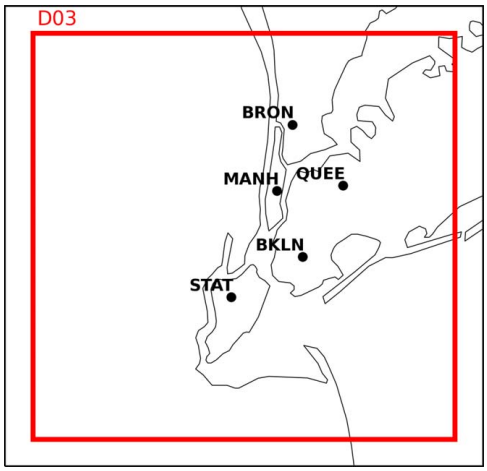

Fig. 6 Weather station locations

Table 4 Heat Index risk categories and ranges

Risk classification	Heat index range (°F)
Very warm	80–90
Hot	90–105
Very hot	105–130
Extremely hot	>130

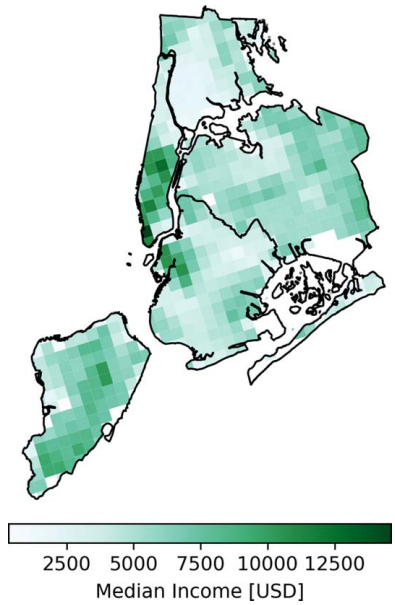

Fig. 7 Five-year medium household income: estimated from the 2017 ACS, interpolated on the WRF 1-km domain

indoor occupational exposure to heat and hot environments [56,57]. Finally, heat exposure hours were computed for each risk category for every grid point in the 1 km NO_AC model run for the summer of 2018. Table 4 shows the Heat Index risk categories used for this study.

We also estimate the energy burden associated with the cost of AC operations during the summer of 2018 using an energy burden metric that is a function of $cost_{AC,household}$ and the $Income_{household}$ as follows:

$$Energy_{Burden} = \frac{cost_{AC,household}}{Income_{household}} \tag{7}$$

Here, the $cost_{AC,household}$ is the cost of electricity during the summer as a function of AC electricity use for cooling. This value was derived using the CURRENT_AC case on a 1 km × 1 km grid point scale that resolves how much AC is used in terms of kW/m^2. AC cost per kWh was obtained from Consolidated Edison (ConEd), the primary energy service provider in the NYC region, by using the schedule 2 ConEd rate at the residential scale for the

Table 5 Model evaluation metrics

	Temperature			Wind direction			Wind speed		
Stations	R^2	RMSE	MAE	R^2	RMSE	MAE	R^2	RMSE	MAE
BKLN	66%	3.02	2.34	32%	76.38	45.74	34%	1.64	1.31
BRON	74%	2.80	2.16	17%	99.11	57.68	34%	1.14	0.89
MANH	74%	2.76	2.17	20%	94.86	57.43	7%	1.39	1.08
QUEE	65%	3.20	2.54	25%	84.73	47.57	37%	1.47	1.14
STAT	72%	2.93	2.28	21%	87.61	50.09	45%	1.88	1.47
Average	70%	2.94	2.30	23%	88.54	51.70	31%	1.50	1.18

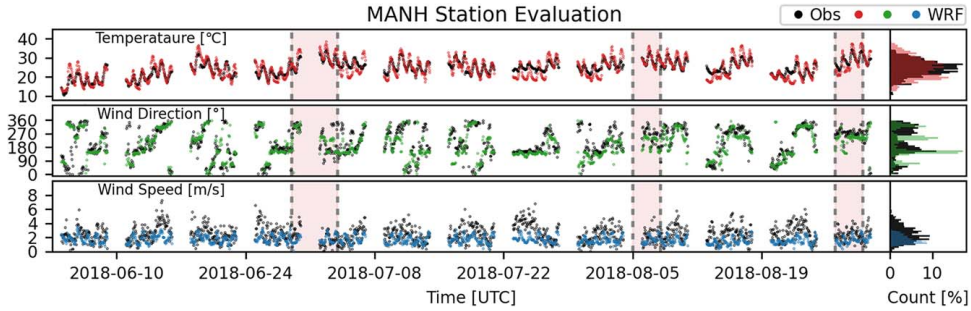

Fig. 8 Manhattan time series of model and observation used for evaluation

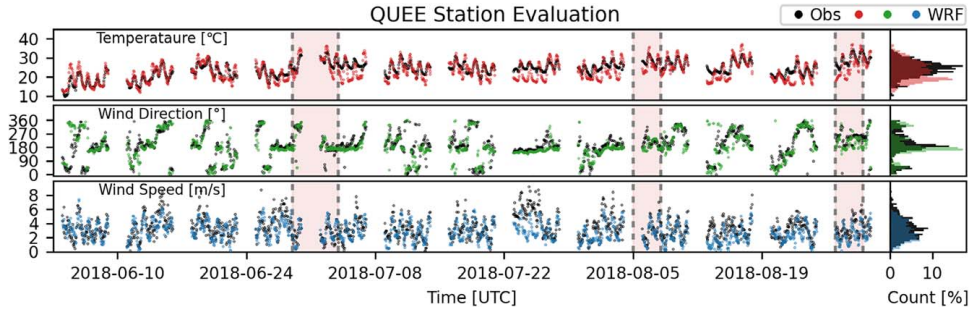

Fig. 9 Queens time series of model and observation used for evaluation

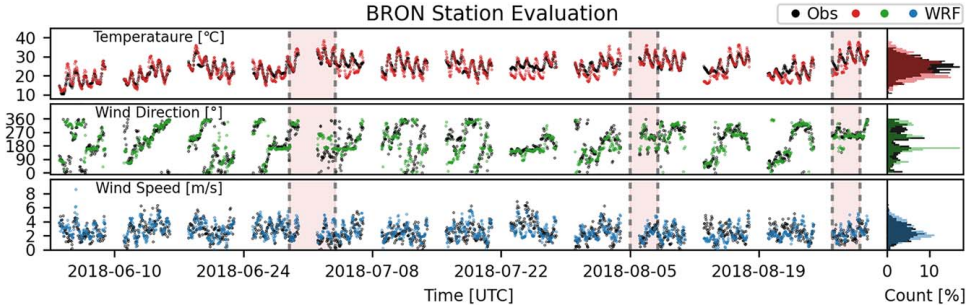

Fig. 10 Bronx time series of model and observation used for evaluation

2018 summer period. The price was 0.2493 US$/kWh for the months of May to September. $Income_{household}$ was then derived from the American Community Survey (ACS) 2017 5-year estimate with data interpolated to a 1-km resolution to match the uWRF CURRENT_AC domain resolution as shown in Fig. 7.

3 Results

3.1 Model Evaluation. Model performance was evaluated against ground weather station data from the New York State Mesonet network for the entire summer of 2018, and the results of this evaluation are shown in Table 5. Modeled temperatures were compared favorably with observations across every station with an average R^2 value of 70%, average RMSE of 2.94 °C, and average MAE of 2.30 °C. A similar analysis was done for wind direction and wind speed resulting in an average R^2 value of 23%, average RMSE of 89 deg and average MAE of 51 deg for wind direction and an average R^2 value of 31%, average RMSE of 1.5 m/s, and average MAE of 1.18 m/s for wind speed. The months of July and August had a lot more precipitation in comparison with June 2018; thus, an evaluation of the single month of June led to a surface temperature R^2 value of 82%, average RMSE of 2.17 °C, and average MAE of 1.71 °C. These results compare favorably with recent studies in New York City for similar heat wave events [6,40] as well as a recent case study over two major cities in Arizona: Phoenix and Tucson [36] in which the authors evaluated the uWRF system over a 15-d time period of clear sky conditions. A time series comparison between the model outputs and the observed data was also conducted for every weather station used as shown in Figs. 8–12 with an included distribution plot on the right of these figures. The distribution plots compare the range and frequency of the observation data and model results with the bars representing a count percentage of occurrence. The timing of the peak temperature was captured very well across every station with similar performance in tracking the diurnal profile. Figure 8 shows that the model was able to track the dynamic change of temperature during each heatwave in the Manhattan site. The dashed vertical bands in each figure mark the start and end of the respective heatwave event. The model had a tendency to under predict the temperature across each station as well, with the most extreme case happening in the Queens location as shown in Fig. 9. This is highlighted by the associated distribution plot that shows the peak model occurrence shifted lower than the observed temperature occurrence. In terms of wind direction, the time series plot shows that the model did very well in capturing

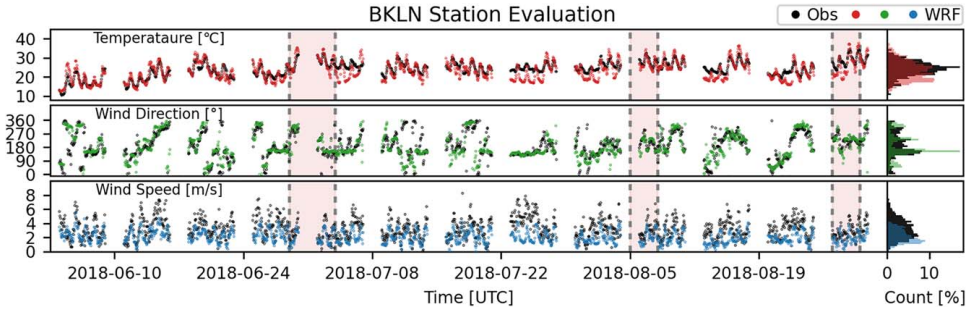

Fig. 11 Brooklyn time series of model and observation used for evaluation

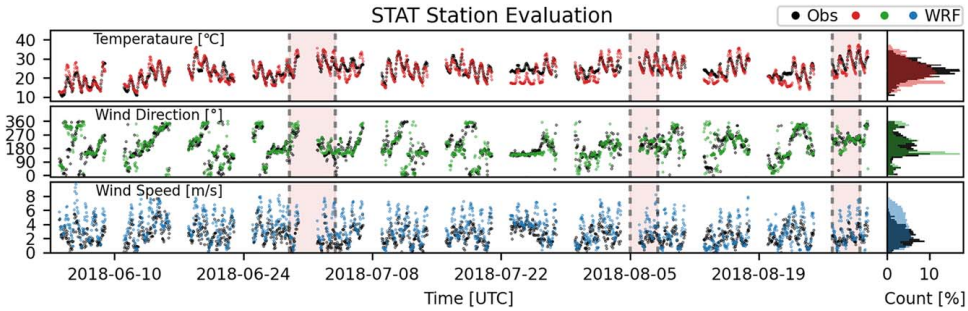

Fig. 12 Staten Island time series of model and observation used for evaluation

the diurnal behavior across every station. The distribution plot also shows that the model was able to capture the multimodal behavior of the distribution. Finally, in terms of wind speed, the model was able to perform very well in the Queens (Fig. 9) and Bronx (Fig. 10) site with a very similar distribution in comparison with the observed wind speed. For the Manhattan (Fig. 8) and Brooklyn (Fig. 11) sites, the model tended to underpredict the wind speed while the model overpredicted the wind speed in the final Staten Island (Fig. 12) location.

A surface plot showing the model outputs for four different times during one of the 2018 heatwaves (Aug. 6, 2018) is also shown in Fig. 13. Here, the five surface observations were overlaid on the plot to explore the spatial performance of the model, including observed wind as shown by the bolded wind barbs and the surface temperature with corresponding error overlaid in text. From these results, it is shown that the model was able to capture the low winds and surface temperature at 14:00 UTC (Fig. 13(*a*)) well at each station. As time progressed, the model was able to capture the dynamic behavior of the wind, especially in the Brooklyn region in which the observed wind direction and wind speed matched the model at every time-step. Although the model captured the stagnant air during the peak heat period of 18:00 UTC (Fig. 13(*c*)) in the Bronx and Manhattan regions, the model tended to overpredict the peak surface temperature. These errors were then reduced at the 20:00 UTC (Fig. 13(*d*)) mark, as the model performed very well in terms of temperature and wind.

3.2 Socioeconomic Impacts. The NO_AC uWRF case was used to estimate the indoor heat exposure level for the population of people who had no access to AC. Figure 14 shows a set of spatial indoor air temperature plots at four different times during the same day (Aug. 6, 2018). At 14:00 UTC (Fig. 14(*a*)), the average ambient air temperature was about 29 °C while the average indoor air temperature was about 38 °C across the entire domain. Although the indoor air temperature was relatively uniform across the domain during this time, the Bronx region experienced a slightly higher indoor air temperature of about 4 °C. As the time progressed to 20:00 UTC (Fig. 14(*c*)), average ambient air temperature was about 33 °C while average indoor air temperature was about 46 °C across the entire domain. The increase in indoor air temperature was noticeably higher in the same Bronx region in comparison to the earlier 14:00 UTC time with an

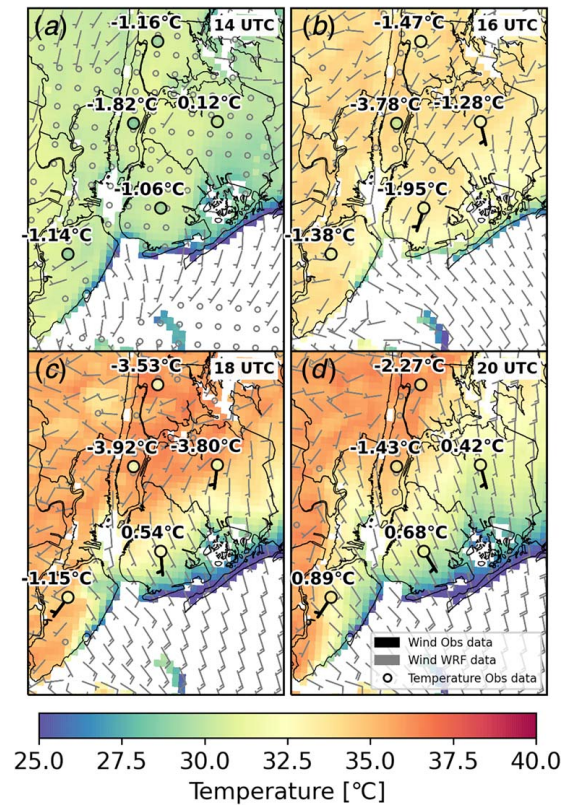

Fig. 13 Surface plot of model and surface station data during Aug. 6, 2018 heatwave: circles represent temperature observations, bolded wind barbs represent surface observation

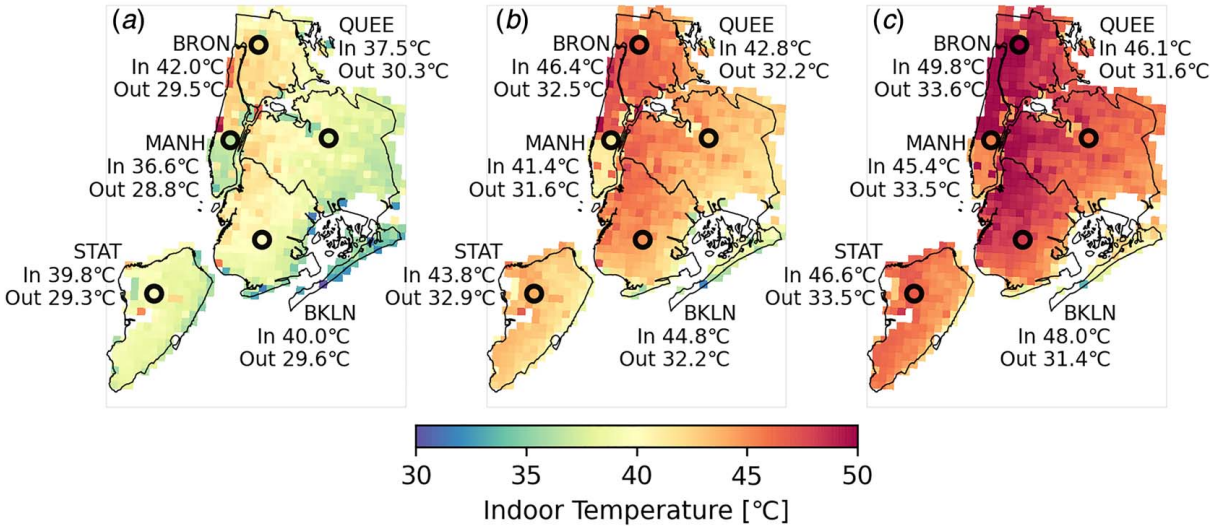

Fig. 14 Model indoor air temperature surface plot during Aug. 6, 2018 heatwave

indoor air temperature condition of about 49 °C, the highest temperature in comparison to the other four boroughs. The Brooklyn location had the second highest indoor air temperature at 20:00 UTC but also experienced the highest change in comparison to the ambient outside air temperature with a delta of about 17 °C. Lower Manhattan experienced the coolest indoor temperatures throughout the four time periods, which is expected with its highest AC % in the domain. The lower Queens area also had a cooler indoor temperature at 20:00 UTC, which did not seem to change much as time progressed. This can potentially be explained by the large amounts of sea breeze wind it experienced during the 16:00–20:00 UTC time as shown in the previous Fig. 13. The relatively high indoor temperatures simulated are likely due to the minimum natural ventilation that uWRF can represent retaining most of the energy within the building envelope. However, very warm conditions were reported from actual indoor measurements in mid-rise residential conditions in NYC by Vant-Hull et al. [54]. A similar study in Detroit, MI, found that maximum indoor temperatures were an average of 13.8 °C warmer than outdoor temperatures [58].

We quantify extreme heat hazard using total number of hours exposed to dangerous levels of heat index using the NO_AC case (Fig. 15). These results show the spatial variability of hours exposed to heat in terms of heat index, grouped into four different plots defined by the NWS risk category for the entire summer of 2018. The first risk group, labeled VERY WARM (Fig. 15(*a*)), had low amounts of exposure in terms of hours with total hours less than 500 across the entire domain. The second risk group labeled HOT (Fig. 15(*b*)) had a similar geospatial pattern in comparison to the VERY WARM case, but with an increased intensity of exposure to about 900 h. The primary feature between these two categories included the peak intensity surrounding the midtown/downtown Manhattan region. The following risk group labeled VERY HOT (Fig. 15(*c*)), on the other hand, experienced the highest numbers of exposed hours across the entire domain. This is clearly shown in Fig. 15(*c*), where regions in upper Manhattan and the Bronx were exposed to more than 1300 h of VERY HOT heat. The final risk group labeled EXTREMELY HOT (Fig. 15(*d*)) had a similar geospatial pattern in comparison with that labeled the VERY HOT case, but had a much lower intensity of exposure to about 300 h. The final two cases have a stark shift in exposure level in contrast to the first two risk levels of VERY WARM and HOT that includes peak intensities surrounding the Manhattan region. The heat index exposure ended up shifting toward the lower income regions like uptown Manhattan and South Bronx in comparison with lower Manhattan where the exposed hours to VERY HOT conditions dropped to nearly zero.

CURRENT_AC results were used to estimate the energy burden associated with the cost of AC operations during the summer of 2018 and are presented in Fig. 16. Results show that the AC burden had a peak of about 0.020% of total income per cooled square meter in areas like the South Bronx and Central/Eastern Brooklyn (boundaries highlighted in Fig. 16), while also coinciding with regions of low AC adoption rates, low household incomes, and peak heat exposure hours. These results highlight some of the trade-

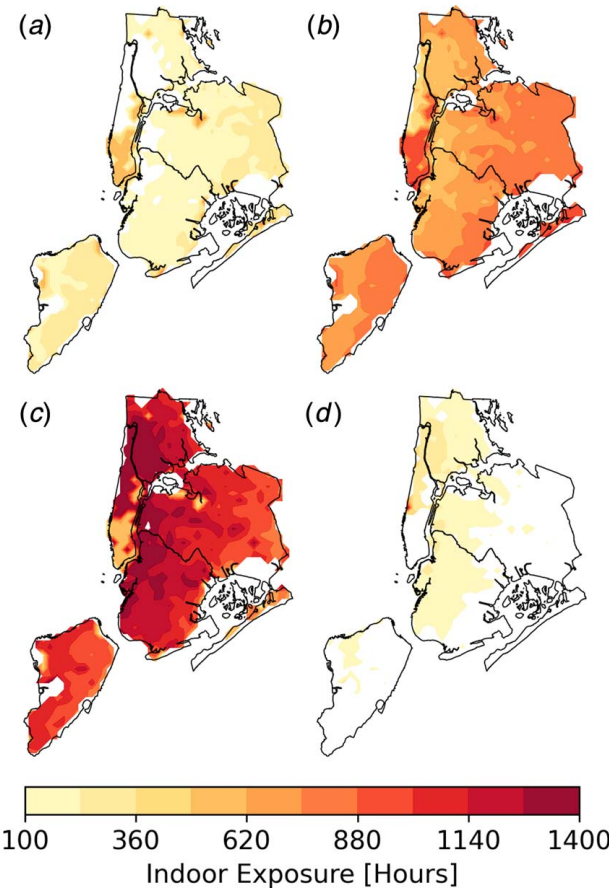

Fig. 15 Number of hours of indoor exposure: for (*a*) very warm, (*b*) hot, (c) very hot, and (*d*) extremely hot heat index conditions

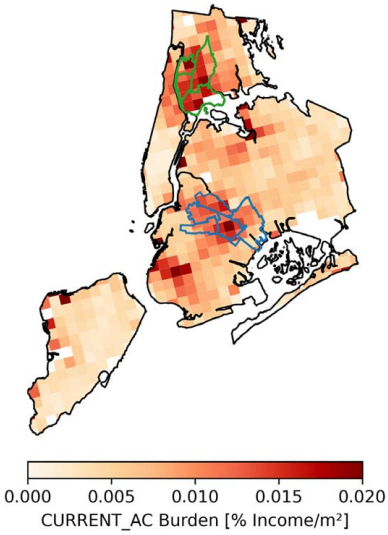

Fig. 16 AC utility cost burden: upper bounday represents South Bronx region, while lower boundary represents EAST and Central Brooklyn

offs involved in the discussion of heat adaptation measures. Although low-income neighborhoods experience the longest exposure time to indoor heat, they also see the highest relative costs of AC operation.

3.3 Environmental Impacts. The CURRENT_AC case and FULL_AC case were used to explore the environmental impacts on the domain if we assume that 100% AC was used to cool every building in NYC and maintain a temperature of 23 °C. In this study, the increase in adoption was attributed in residential land classes, which impacts the sensible heat flux from AC systems into the environment, while latent heat fluxes remain constant (attributed to commercial sites). As such, Fig. 17 shows the sensible heat flux released into the environment as a result of the AC use for each case during a heat wave in NYC. While Manhattan maintained a similar peak across both cases, there was a noticeable increase across every borough, especially within the regions that previously had a low percentage of AC. Taking for example upper Manhattan and the Bronx, from Fig. 17(*c*), there was an additional 65 W/m^2 of sensible heat flux released into the environment due to the AC adoption. When looking at downtown Manhattan and Staten Island, there was not much of a change.

This trend was also evident when looking into how the UHI was affected due to the additional AC. Figure 18 shows a spatial plot of the temperature difference between the FULL_AC case and the CURRENT_AC case. Here, higher values represent a hotter ambient temperature within the environment due to the additional heat released by the FULL_AC case. Regions like the Bronx and central Queens experienced a peak of about 1.1 °C and 0.9 °C, respectively, during this heatwave following the spatial trend presented by the heat flux plot in Fig. 17. A time series plot was also used to explore how this temperature difference varied throughout the summer of 2018 and is presented in Fig. 19. Here, two different locations were chosen to contrast the differences of AC adoption. The Bronx location had an AC adoption of about 75% while the Staten island location had an AC adoption of about 95%. During the first heatwave as shown in Fig. 19, the temperature difference hit a peak difference of about 2.50 °C in the Bronx and about 1.50 °C for Staten Island. The Bronx location also had a much higher spread of temperature differences as shown by the histogram plot to the right of Fig. 19. The Bronx location had a wider range between 1.00 °C and −1.00 °C as compared to the Staten island case, which fell between 0.50 °C and −0.50 °C.

3.4 Infrastructure Impacts. The CURRENT_AC case and FULL_AC case were used to explore the impacts on infrastructure based on the increased peak energy demand brought on by 100% AC in NYC. Figure 20 shows the total city-scale load (MW) during the three heat wave events from 2018. The CURRENT_AC case had an average peak of about 9000 MW during the most intense points of each heat wave. The FULL_AC case, on the other hand, had an average increase of about 20% with a peak reaching 10750 MW on July 2, 2018 and August 29, 2018. Figure 21 shows the spatial distribution of AC electrical consumption in terms of W/m^2 for every grid point across the NYC domain during the second heat wave event. From The CURRENT_AC case shown in Fig. 21(*a*), Manhattan had the highest consumption of about 55 W/m^2. Areas with very low AC adoption had an average load of about 4 W/m^2 as evident in the Bronx and Queens location point on Fig. 21. With the FULL_AC case as shown in Fig. 21(*b*), there was a drastic difference in these two locations with a 300–500% increase, respectively. The moderate AC case shown by the Brooklyn location with 93% AC experienced an increase consumption of about 50% while the Manhattan site stayed relatively the same. These results can be further verified by

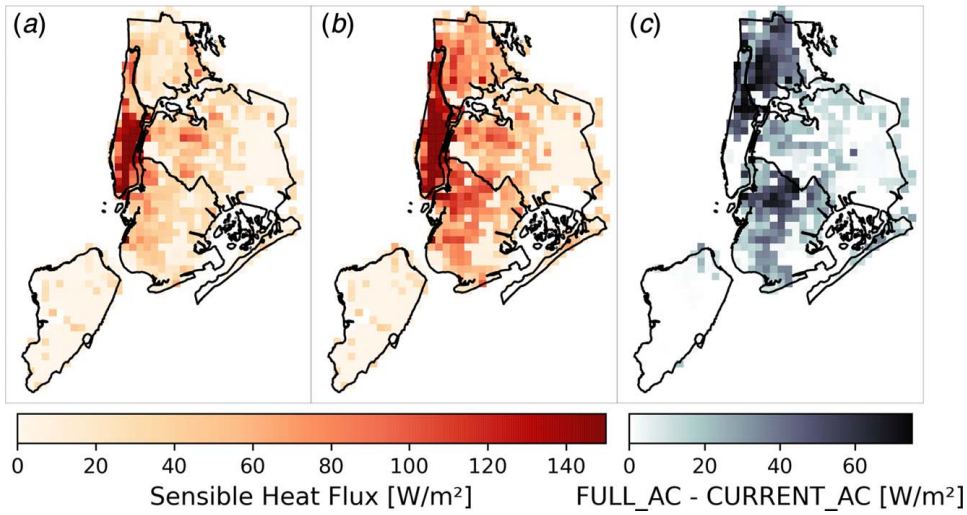

Fig. 17 Spatial plot of model-sensible heat flux for (*a*) CURRENT_AC, (*b*) FULL_AC case, and (*c*) difference between both (*a*) and (*b*)

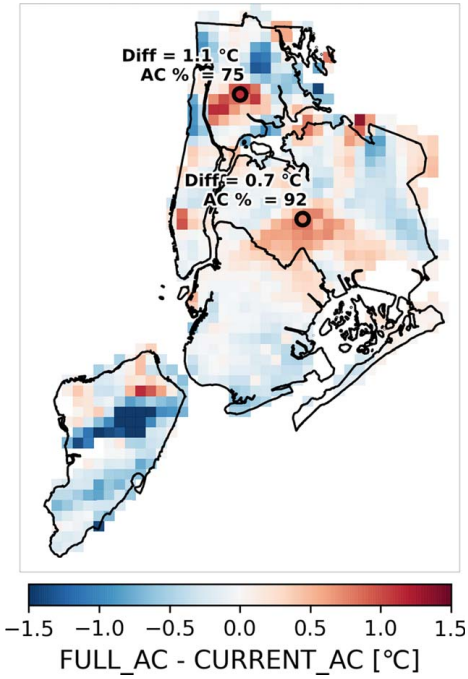

Fig. 18 Model temperature comparison: temperature difference between FULL_AC case and CURRENT_AC case

Fig. 22 in which the percent difference between the two cases was plotted for the early August heat wave. The Manhattan site had no change during this heat wave while the Bronx location with an AC % difference of 24% had a peak increase of about 550%. This is an expected result as Manhattan has most high-rise buildings with the current highest percentage of AC in the buildings.

4 Conclusions

This work explored the impact of increasing residential AC system adoption to 100% as an adaptive measure to reduce human health risks under heat waves in NYC. This study used AC adoption data from the 2017 New York City Housing and Vacancy Survey to study impacts to health, energy demand, and UHI. A mesoscale WRF model was chosen and coupled with the multilayer building environment parameterization and building energy model (BEP–BEM) to provide an appropriate urban climate modeling framework to investigate these questions.

Three different case setups were used to evaluate the impacts of going to full AC adoption of 100%. The NO_AC case presented results associated with regions that currently had no AC to highlight the current health risks associated with extended heat exposure. The second CURRENT_AC adoption case used the data from the NYC Housing and Vacancy Survey 2017 to represent the current AC adoption rate in NYC. The final Full_AC adoption case represented the 100% AC adoption case in NYC.

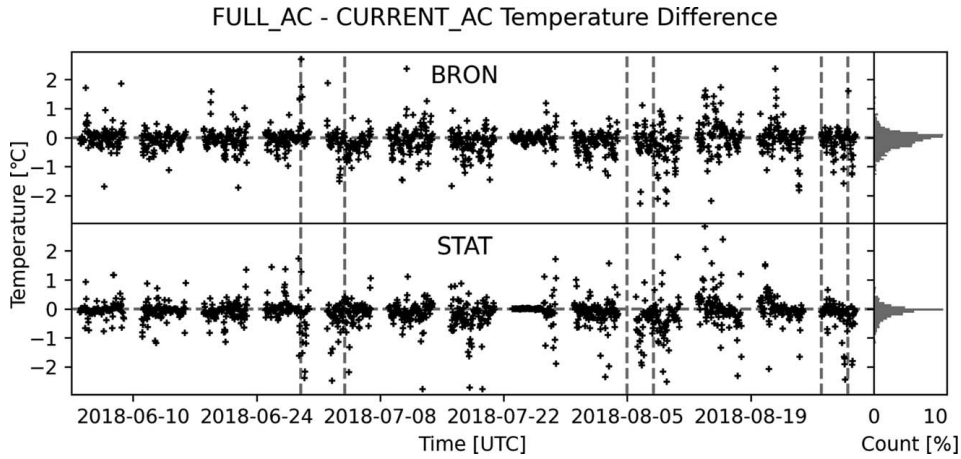

Fig. 19 Model temperature difference time series: temperature time series difference between FULL_AC case and CURRENT_AC case at two different point

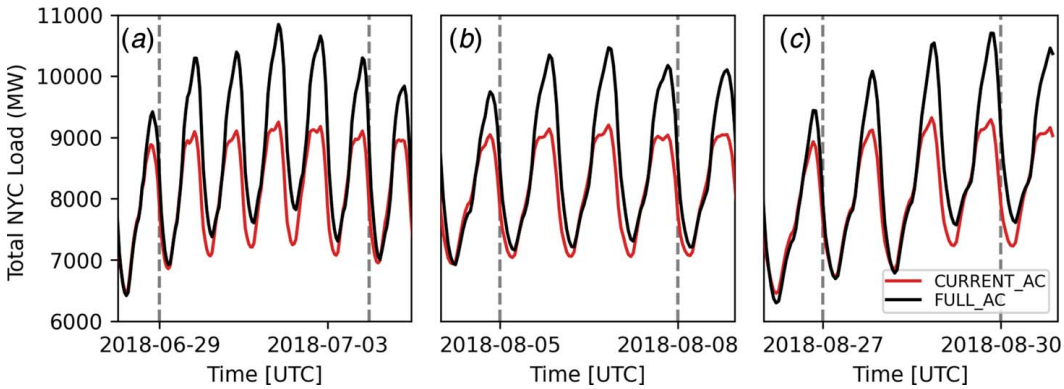

Fig. 20 Total NYC Load for three heat waves: total NYC load for FULL_AC case and CURRENT_AC case during three heat wave events

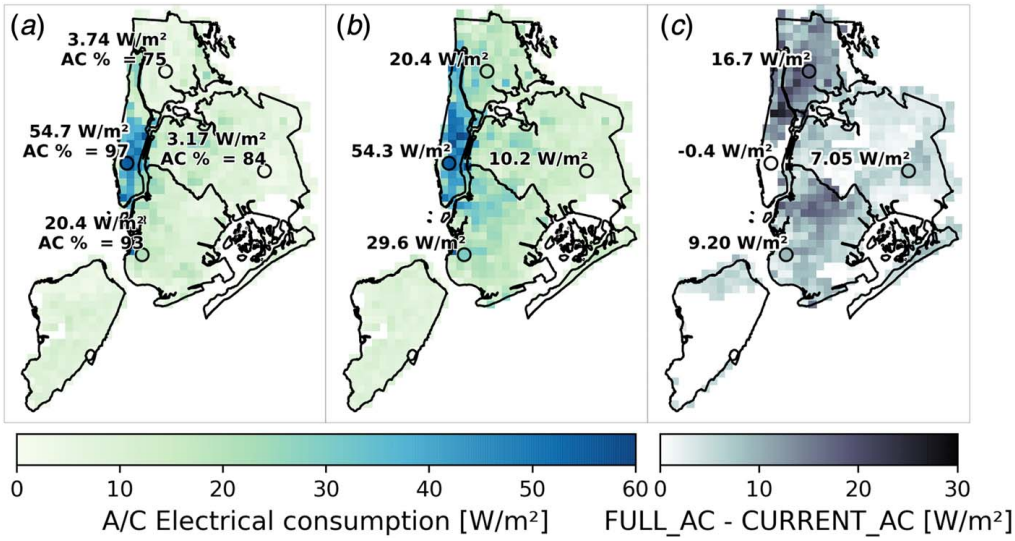

Fig. 21 Spatial plot of AC consumption: spatial plot of AC consumption for (*a*) CURRENT_AC, (*b*) FULL_AC case, and (*c*) difference between both (*a*) and (*b*)

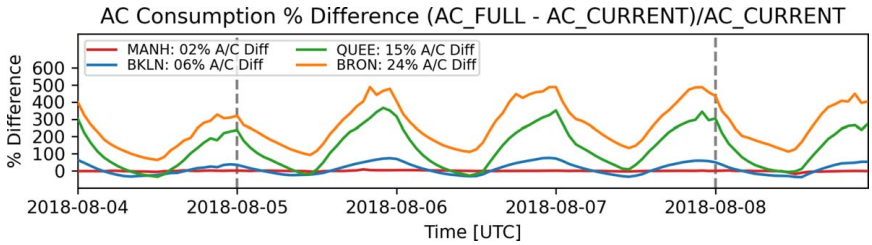

Fig. 22 AC load percent difference between FULL_AC case and CURRENT_AC case during the early August heat wave event at four different locations with different AC percentages

A detailed model evaluation was first performed on the CURRENT_AC adoption case which showed that the uWRF system compared favorably in terms of surface temperature with observations across every station with an average R^2 value of 70%, average RMSE of 2.9 °C, and average MAE of 2.3 °C. As time progressed, the model was also able to capture the dynamic behavior of the wind, especially in the Brooklyn region, with matching observed wind direction and wind speed with the model at every time-step.

To quantify the exposure to extreme heat, the NO_AC case was used to estimate the total number of hours exposed to different levels of indoor heat index. Results showed that regions in upper Manhattan and the Bronx had been exposed to more than 1300 h of VERY HOT heat. There was also a shift toward lower income regions like uptown Manhattan and the South Bronx in comparison with lower Manhattan in which the exposed hours to VERY HOT conditions dropped to nearly zero. The CURRENT_AC case was used to estimate the energy burden associated with the cost of AC operations during the summer of 2018. Results showed that the AC burden had a peak of about 0.020% of total income per cooled square meter in regions coinciding with low AC adoption rates, low household incomes, and peak heat exposure hours. These results highlight some of the trade-offs involved in the discussion of heat adaptation measures. Although low-income neighborhoods experience the longest exposure time to indoor heat, they also see the highest relative costs of AC operation.

The CURRENT_AC case and FULL_AC case were used to explore the environmental and infrastructural impact on the domain if we supposed that 100% AC was used to cool every building in NYC. During the first heatwave in the study timeframe, the temperature difference hit a peak difference of about 2.50 °C in the Bronx and about 1.50 °C for Staten Island. Increases over The Bronx may be particularly important, as studies have shown the core of the daytime UHI to occur over it [6,59]. In terms of energy consumption, The FULL_AC case had an average increase of about 20% with a peak reaching 10750 MW on July 2, 2018 and August 29, 2018. This additional electric load may have necessitated significant investments to upgrade and maintain low-adoption neighborhoods. For example, in July 2019, when neighborhoods in Brooklyn and Queens experienced higher than expected electric loads during a heat wave, the electric utility shut off their power to prevent hardware damage, leaving thousands without power on one of the hottest days of the year [60]. Increasing AC use in lower adoption neighborhoods will increase the likelihood of this type of failure unless utilities commit significant resources to prevent them. Nevertheless, our study shows the different impacts associated with 100% AC and can serve as a guideline when determining policy changes that affect the low-income communities and most vulnerable.

Acknowledgment

This study is supported and monitored by The National Oceanic and Atmospheric Administration—Cooperative Science Center for Earth System Sciences and Remote Sensing Technologies under the Cooperative Agreement (Grant No. NA16SEC4810008). The authors would like to thank The City College of New York, NOAA Center for Earth System Sciences and Remote Sensing Technologies, and NOAA Office of Education, Educational

Partnership Program for fellowship support to Harold Gamarro. The statements contained within the manuscript/research article are not the opinions of the funding agency or the U.S. government, but reflect the author's opinions. This research is also made possible by the New York State (NYS) Mesonet. Original funding for the NYS Mesonet was provided by Federal Emergency Management Agency grant FEMA-4085-DR-NY, with the continued support of the NYS Division of Homeland Security & Emergency Services; the state of New York; the Research Foundation for the State University of New York (SUNY); the University at Albany, SUNY; the Atmospheric Sciences Research Center (ASRC) at SUNY Albany; and the Department of Atmospheric and Environmental Sciences (DAES) at SUNY Albany. Additional support was provided by Urban Resilience to Extreme Weather-Related Events Sustainability Research Network (UREx SRN; NSF Grant No. 1444755).

References

[1] Hoegh-Guldberg, O., Jacob, D., Taylor, M., Bindi, M., Brown, S., Camilloni, I., Diedhiou, A., Djalante, R., Ebi, K., Engelbrecht, F., Guiot, J., Hijioka, Y., Mehrotra, S., Payne, A., Seneviratne, S. I., Thomas, A., Warren, R., and Zhou, G., 2018, "Impacts of 1.5 °C Global Warming on Natural and Human Systems," *Global Warming of 1.5 °C. An IPCC Special Report on the Impacts of Global Warming of 1.5 °C Above Pre-Industrial Levels and Related Global Greenhouse Gas Emission Pathways, in the Context of Strengthening the Global Response to the Threat of Climate Change, Sustainable Development, and Efforts to Eradicate Poverty*, V. Masson-Delmotte, P. Zhai, H.-O. Pörtner, D. Roberts, J. Skea, P. R. Shukla, A. Pirani, W. Moufouma-Okia, C. Péan, R. Pidcock, S. Connors, J. B. R. Matthews', Y. Chen, X. Zhou, M. I. Gomis, E. Lonnoy, T. Maycock, M. Tignor, and T. Waterfield, eds., in press, https://www.ipcc.ch/sr15/chapter/chapter-3/

[2] Hamstead, Z. A., Farmer, C., and McPhearson, T., 2018, "Landscape-Based Extreme Heat Vulnerability Assessment," J. Extrem. Events., **5**(4), p. 1850018.

[3] Wong, K. V., Paddon, A., and Jimenez, A., 2013, "Review of World Urban Heat Islands: Many Linked to Increased Mortality," ASME J. Energy Resour. Technol., **135**(2), p. 022101.

[4] González, J. E., Ortiz, L., Smith, B. K., Devineni, N., Colle, B., Booth, J. F., Ravindranath, A., Rivera, L., Horton, R., Towey, K., Kushnir, Y., Manley, D., Bader, D., and Rosenzweig, C., 2019, "New York City Panel on Climate Change 2019 Report Chapter 2: New Methods for Assessing Extreme Temperatures, Heavy Downpours, and Drought," Ann. N. Y. Acad. Sci., **1439**(1), pp. 30–70.

[5] Tan, J., Zheng, Y., Tang, X., Guo, C., Li, L., Song, G., Zhen, X., Yuan, D., Kalkstein, A. J., Li, F., and Chen, H., 2010, "The Urban Heat Island and Its Impact on Heat Waves and Human Health in Shanghai," Int. J. Biometeorol., **54**(1), pp. 75–84.

[6] Ortiz, L. E., Gonzalez, J. E., Wu, W., Schoonen, M., Tongue, J., and Bornstein, R., 2018, "New York City Impacts on a Regional Heat Wave," J. Appl. Meteorol. Climatol., **57**(4), pp. 837–851.

[7] Oke, T. R., 1973, "City Size and the Urban Heat Island," Atmos. Environ., **7**(8), pp. 769–779.

[8] Oke, T. R., 1982, "The Energetic Basis of the Urban Heat Island," Q. J. R. Meteorol. Soc., **108**(455), pp. 1–24.

[9] Arnfield, A. J., 2003, "Two Decades of Urban Climate Research: A Review of Turbulence, Exchanges of Energy and Water, and the Urban Heat Island," Int. J. Climatol., **23**(1), pp. 1–26.

[10] Li, D., and Bou-Zeid, E., 2013, "Synergistic Interactions Between Urban Heat Islands and Heat Waves: The Impact in Cities Is Larger Than the Sum of Its Parts," J. Appl. Meteorol. Climatol., **52**(9), pp. 2051–2064.

[11] Founda, D., and Santamouris, M., 2017, "Synergies Between Urban Heat Island and Heat Waves in Athens (Greece), During an Extremely Hot Summer (2012)," Sci. Rep., **7**(1), pp. 10973.

[12] Ramamurthy, P., González, J., Ortiz, L., Arend, M., and Moshary, F., 2017, "Impact of Heatwave on a Megacity: An Observational Analysis of New York City During July 2016," Environ. Res. Lett., **12**(5), p. 054011.

[13] Ao, X., Wang, L., Zhi, X., Gu, W., Yang, H., and Li, D., 2019, "Observed Synergies Between Urban Heat Islands and Heat Waves and Their Controlling Factors in Shanghai, China," J. Appl. Meteorol. Climatol., **58**(9), pp. 1955–1972.

[14] Santamouris, M., 2020, "Recent Progress on Urban Overheating and Heat Island Research. Integrated Assessment of the Energy, Environmental, Vulnerability and Health Impact. Synergies with the Global Climate Change," Energy Build., **207**(1), pp. 109482.

[15] Ramamurthy, P., and Bou-Zeid, E., 2017, "Heatwaves and Urban Heat Islands: A Comparative Analysis of Multiple Cities," J. Geophys. Res., **122**(1), pp. 168–178.

[16] Arent, D. J., Tol, R. S. J., Faust, E., Hella, J. P., Kumar, S., Strzepek, K. M., Tóth, F. L., and Yan, D., 2014, "Key Economic Sectors and Services," *Climate Change 2014: Impacts, Adaptation, and Vulnerability. Part A: Global and Sectoral Aspects. Contribution of Working Group II to the Fifth Assessment Report of the Intergovernmental Panel on Climate Change*, C. B. Field, V. R. Barros, D. J. Dokken, K. J. Mach, M. D. Mastrandrea, T. E. Bilir, M. Chatterjee, K. L. Ebi, Y. O. Estrada, R. C. Genova, B. Girma, E. S. Kissel, A. N. Levy, S. MacCracken, P. R. Mastrandrea, and L. L. White, eds., Cambridge University Press, Cambridge, UK/New York, NY, pp. 659–708. https://www.ipcc.ch/site/assets/uploads/2018/02/WGIIAR5-Chap10_FINAL.pdf

[17] Hong, J., and Kim, W. S., 2015, "Weather Impacts on Electric Power Load: Partial Phase Synchronization Analysis," Meteorol. Appl., **22**(4), pp. 811–816.

[18] International Energy Agency (IEA), 2018, *The Future of Cooling: Opportunities for Energy-Efficient Air Conditioning*, IEA, Paris.

[19] United Nations, 2019, *World Population Prospects 2019: Highlights*, United Nations, New York.

[20] United Nations: Department of Economic and Social Affairs, 2019, *World Urbanization Prospects: The 2018 Revision*, UN, New York.

[21] Santamouris, M., 2016, "Cooling the Buildings—Past, Present and Future," Energy Build., **128**(1), pp. 617–638.

[22] Knowlton, K., Lynn, B., Goldberg, R. A., Rosenzweig, C., Hogrefe, C., Rosenthal, J. K., and Kinney, P. L., 2007, "Projecting Heat-Related Mortality Impacts Under a Changing Climate in the New York City Region," Am. J. Public Health., **97**(11), pp. 2028–2034.

[23] Rosenthal, J.K., Kinney, P. L., and Metzger, K. B., 2014, "Intra-Urban Vulnerability to Heat-Related Mortality in New York City, 1997–2006," Health & Place, **30**(1), pp. 45–60.

[24] Madrigano, J., Ito, K., Johnson, S., Kinney, P. L., and Matte, T., 2015, "A Case-Only Study of Vulnerability to Heat Wave–Related Mortality in New York City (2000–2011)," Environ. Health Perspect., **123**(7), pp. 672–678.

[25] Smoyer, K. E., 1998, "Putting Risk in Its Place: Methodological Considerations for Investigating Extreme Event Health Risk," Soc. Sci. Med., **47**(11), pp. 1809–1824.

[26] Kolokotsa, D., and Santamouris, M., 2015, "Review of the Indoor Environmental Quality and Energy Consumption Studies for Low Income Households in Europe," Sci. Total Environ., **536**(1), pp. 316–330.

[27] O'Neill, M. S., Zanobetti, A., and Schwartz, J., 2005, "Disparities by Race in Heat-Related Mortality in Four US Cities: The Role of Air Conditioning Prevalence," J. Urban Heal., **82**(2), pp. 191–197.

[28] Ito, K., Lane, K., and Olson, C., 2018, "Equitable Access to Air Conditioning: A City Health Department's Perspective on Preventing Heat-Related Deaths," Epidemiology, **29**(6), pp. 749–752.

[29] Kontokosta, C. E., Reina, V. J., and Bonczak, B., 2020, "Energy Cost Burdens for Low-Income and Minority Households: Evidence From Energy Benchmarking and Audit Data in Five U.S. Cities," J. Am. Plan. Assoc., **86**(1), pp. 89–105.

[30] Skamarock, W. C., Klemp, J. B., Dudhi, J., Gill, D. O., Barker, D. M., Duda, M. G., Huang, X.-Y., Wang, W., and Powers, J. G., 2008, *A Description of the Advanced Research WRF version 3*, NCAR Tech. Note NCAR/TN–475+STR, National Center for Atmospheric Research, Boulder, CO.

[31] Salamanca, F., Krpo, A., Martilli, A., and Clappier, A., 2010, "A New Building Energy Model Coupled with an Urban Canopy Parameterization for Urban Climate Simulations-Part I. Formulation, Verification, and Sensitivity Analysis of the Model," Theor. Appl. Climatol., **99**(3–4), pp. 331–344.

[32] Salamanca, F., Georgescu, M., Mahalov, A., Moustaoui, M., Wang, M., and Svoma, B. M., 2013, "Assessing Summertime Urban Air Conditioning Consumption in a Semiarid Environment," Environ. Res. Lett., **8**(3), p. 034022.

[33] Gutiérrez, E., González, J. E., Bornstein, R., Arend, M., and Martilli, A., 2013, "A New Modeling Approach to Forecast Building Energy Demands During Extreme Heat Events in Complex Cities," ASME J. Sol. Energy Eng., **135**(4), p. 040906.

[34] Ortiz, L. E., Gonzalez, J. E., Gutierrez, E., and Arend, M., 2016, "Forecasting Building Energy Demands With a Coupled Weather-Building Energy Model in a Dense Urban Environment," ASME J. Sol. Energy Eng., **139**(1), p. 011002.

[35] Takane, Y., Kikegawa, Y., Hara, M., Ihara, T., Ohashi, Y., Adachi, S. A., Kondo, H., Yamaguchi, K., and Kaneyasu, N., 2017, "A Climatological Validation of Urban Air Temperature and Electricity Demand Simulated by a Regional Climate Model Coupled with an Urban Canopy Model and a Building Energy Model in an Asian Megacity," Int. J. Climatol., **37**(S1), pp. 1035–1052.

[36] Salamanca, F., Zhang, Y., Barlage, M., Chen, F., Mahalov, A., and Miao, S., 2018, "Evaluation of the WRF-Urban Modeling System Coupled to Noah and Noah-MP Land Surface Models Over a Semiarid Urban Environment," J. Geophys. Res. Atmos., **123**(5), pp. 2387–2408.

[37] Xu, X., González, J. E., Shen, S., Miao, S., and Dou, J., 2018, "Impacts of Urbanization and Air Pollution on Building Energy Demands—Beijing Case Study," Appl. Energy., **225**(1), pp. 98–109.

[38] Oke, T. R., 1987, *Boundary Layer Climates*, 2nd ed., Matheuen, London.

[39] Martilli, A., 2002, "Numerical Study of Urban Impact on Boundary Layer Structure: Sensitivity to Wind Speed, Urban Morphology, and Rural Soil Moisture," J. Appl. Meteorol, **41**(12), pp. 1247–1266.

[40] Gutiérrez, E., González, J. E., Martilli, A., Bornstein, R., and Arend, M., 2015, "Simulations of a Heat-Wave Event in New York City Using a Multilayer Urban Parameterization," J. Appl. Meteorol. Climatol., **54**(2), pp. 283–301.

[41] Ortiz, L. E., González, J. E., Horton, R., Lin, W., Wu, W., Ramamurthy, P., Arend, M., and Bornstein, R. D., 2019, "High-Resolution Projections of Extreme Heat in New York City," Int. J. Climatol., **39**(12), pp. 4721–4735.

[42] Martilli, A., Clappier, A., and Rotach, M. W., 2002, "An Urban Surface Exchange Parameterisation for Mesoscale Models," Boundary-Layer Meteorol., **104**(2), pp. 261–304.

[43] Gutiérrez, E., González, J. E., Martilli, A., and Bornstein, R., 2015, "On the Anthropogenic Heat Fluxes Using an Air Conditioning Evaporative Cooling Parameterization for Mesoscale Urban Canopy Models," ASME J. Sol. Energy Eng., **137**(5), p. 051005.

[44] Crawley, D. B., Lawrie, L. K., Winkelmann, F. C., Buhl, W. F., Huang, Y. J., Pedersen, C. O., Strand, R. K., Liesen, R. J., Fisher, D. E., Witte, M. J., and Glazer, J., 2001, "EnergyPlus: Creating a New-Generation Building Energy Simulation Program," Energy Build., **33**(4), pp. 319–331.

[45] Salamanca, F., Georgescu, M., Mahalov, A., Moustaoui, M., and Wang, M., 2014, "Anthropogenic Heating of the Urban Environment Due to Air Conditioning," J. Geophys. Res., **119**(10), pp. 5949–5965.
[46] Ortiz, L., González, J. E., and Lin, W., 2018, "Climate Change Impacts on Peak Building Cooling Energy Demand in a Coastal Megacity," Environ. Res. Lett., **13**(9), p. 094008.
[47] Ek, M.B., Mitchell, K.E., Lin, Y., Rogers, E., Grunmann, P., Mitchell, K., Koren, V., Gayno, G., and Tarpley, J.D., 2003, "Implementation of Noah Land Surface Model Advances in the National Centers for Environmental Prediction operational Mesoscale Eta Model," J. Geophys. Res., **108**(D22), p. 8851.
[48] Iacono, M. J., Delamere, J. S., Mlawer, E. J., Shephard, M. W., Clough, S. A., and Collins, W. D., 2008, "Radiative Forcing by Long-Lived Greenhouse Gases: Calculations with the AER Radiative Transfer Models," J. Geophys. Res. Atmos., **113**(D13), p. D13103.
[49] Janjić, Z. I., 1994, "The Step-Mountain Eta Coordinate Model: Further Developments of the Convection, Viscous Sublayer, and Turbulence Closure Schemes," Mon. Weather Rev., **122**(5), pp. 927–945.
[50] Thompson, G., and Eidhammer, T., 2014, "A Study of Aerosol Impacts on Clouds and Precipitation Development in a Large Winter Cyclone," J. Atmos. Sci., **71**(10), pp. 3636–3658.
[51] Steadman, R. G., 1979, "The Assessment of Sultriness. Part I. A Temperature-Humidity Index Based on Human Physiology and Clothing Science," J. Appl. Meteorol., **18**(7), pp. 861–873.
[52] Anderson, G. B., Bell, M. L., and Peng, R. D., 2013, "Methods to Calculate the Heat Index as an Exposure Metric in Environmental Health Research," Environ. Health Perspect., **121**(10), pp. 1111–1119.
[53] American Society of Heating, Refrigerating and Air-Conditioning Engineers, 2017, *2017 ASHRAE Handbook. Fundamentals.*, ASHRAE, Atlanta, GA.
[54] Vant-Hull, B., Ramamurthy, P., Havlik, B., Jusino, C., Corbin-Mark, C., Schuerman, M., Keefe, J., Drapkin, J. K., and Glenn, A. A. , 2018, "The Harlem Heat Project A Unique Media-Community Collaboration to Study Indoor Heat Waves," Bull. Am. Meteorol. Soc., **99**(12), pp. 2491–2506.
[55] Uejio, C. K., Tamerius, J. D., Vredenburg, J., Asaeda, G., Isaacs, D. A., Braun, J., Quinn, A., and Freese, J. P., 2016, "Summer Indoor Heat Exposure and Respiratory and Cardiovascular Distress Calls in New York City, NY, U.S," Indoor Air., **26**(4), pp. 594–604.
[56] Cal/OSHA, 2019, "Heat Illness Prevention in Indoor Places of Employment" [Online]. Available: https://www.dir.ca.gov/dosh/doshreg/Heat-illness-prevention-indoors/
[57] Jacklitsch, B., Williams, W., Musolin, K., Coca, A., Kim, J.-H., and Turner, N., 2016, *NIOSH Criteria for a Recommended Standard: Occupational Exposure to Heat and Hot Environments*, National Institute for Occupational Safety and Health, Cincinnati, OH.
[58] White-Newsome, J. L., Sánchez, B. N., Jolliet, O., Zhang, Z., Parker, E. A., Dvonch, J. T., and O'neill, M. S., 2012, "Climate Change and Health: Indoor Heat Exposure in Vulnerable Populations," Environ. Res., **112**(1), pp. 20–27.
[59] Gedzelman, S. D., Austin, S., Cermak, R., Stefano, N., Partridge, S., Quesenberry, S., and Robinson, D. A., 2003, "Mesoscale Aspects of the Urban Heat Island Around New York City," Theor. Appl. Climatol., **75**(1–2), pp. 29–42.
[60] Gold, M., and McGeehan, P., 2019, "Con Edison Points to Record-Breaking Power Usage to Explain Shutdown," New York Times [Online]. https://www.nytimes.com/2019/07/22/nyregion/brooklyn-power-outage- nyc.html